Project Reports

Salvador Castagnino, Theo Koppenhöfer

March 4, 2023

Project 1

Introduction

This report and the code belonging to it can be found online under [4].

The Benchmark

In the following we use the model of a pendulum attached to a rod which is elastic in the radial direction as described in Task 1. The situation is depicted in figure 1.

This problem leads to the formulation as an ODE

$$\begin{bmatrix} y_1 \\ y_2 \\ y_3 \\ y_4 \end{bmatrix}' = \begin{bmatrix} y_3 \\ y_4 \\ -y_1\lambda(y_1, y_2) \\ -y_2\lambda(y_1, y_2) - 1 \end{bmatrix}$$

with

$$\lambda(y_1, y_2) = k\frac{\|(y_1, y_2)\| - 1}{\|(y_1, y_2)\|} \, .$$

The plot of a numerical solution to this problem for $k = 1$ can be seen in figures 2 3 and 4.

We can calculate the potential, kinetic and approximate the elastic energy with the formulas

$$E_{\text{pot}} = 1 + y_2 \qquad E_{\text{kin}} = \frac{\|(y_3, y_4)\|^2}{2} \qquad E_{\text{elast}} = k\frac{(\|(y_1, y_2)\| - 1)^2}{2} \, .$$

Adding these up we get the approximate total energy

$$E_{\text{tot}} = E_{\text{pot}} + E_{\text{kin}} + E_{\text{elast}} \, .$$

We expect the approximate total energy to be constant which indeed can be seen in Figure 5 for that previously calculated numerical solution. Because of this
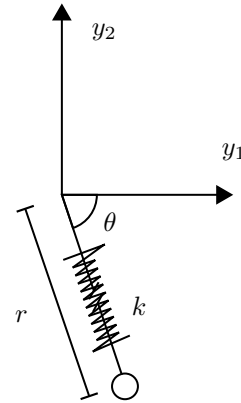
Figure 1: The pendulum

Figure 2: State in dependence of time.

Figure 3: Path traced out by pendulum.

property we can use the variance of the approximate total energy as an index to measure the stability of the method. In the ideal world this index almost vanishes.
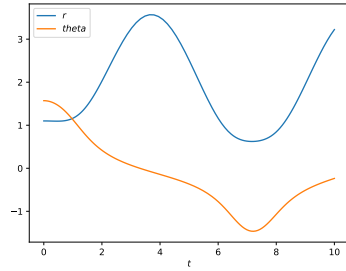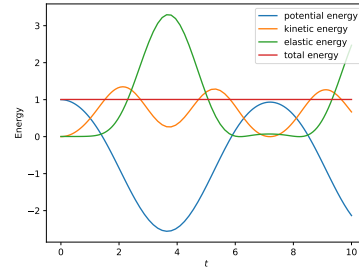

Figure 4: Polar coordinates.

Figure 5: Energy plot

Testing Explicit Methods

For linear problems, explicit methods present a much reduced stability region which dictates the possible step sizes for that specific method. For the problem of the elastic pendulum, approximated by explicit methods, when the value of k is increased we are expected to see the approximation blow up showing oscillations of unbounded amplitude. This unstable behavior will be attenuated by reducing the value of the step h.

The problem was simulated using Explicit Euler and RK4. All the experiments in this section are simulated on the domain $[0, 20]$ and have initial the initial value $y_0 = [1.1, 0, 0, 0]$ if not otherwise stated. The graphs are presented in polar coordinates where r refers to the length of the spring and θ refers to the angle conformed between the pendulum and the vertical axis.
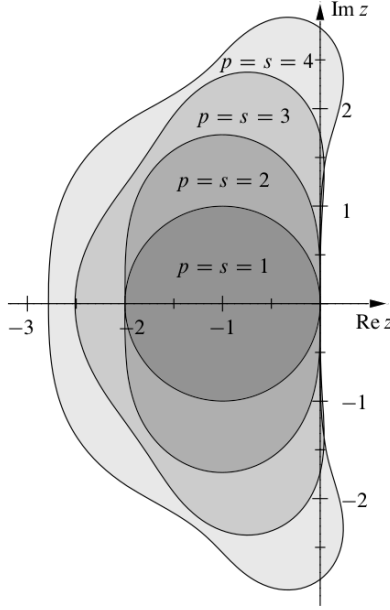
Figure 6: Stability regions of the Runge-Kutta-methods, taken from [2][p.238]

It can be observed that for a step size of $h = 0.01$ Explicit Eurler (Figure 7) already shows instability for values of $k = 50$ while RK4 (Figure 8) with that same step size remains stable for values up to $k = 3000$.

For Explicit Euler (Figure 9), by keeping the value of k constant and reducing the step size by a decimal place we can see how the instability is attenuated presenting a similar amplitude over time. It takes a much larger step size and spring constant for RK4 to become unstable (Figure 10), once unstabilized it's growth is much more rapid than Explicit Euler's and it does so without oscillating.

It is interesting to observe that the oscillation of the spring is rapidly dumped when using RK4 (Figure 11), a behavior similar to that presented by implicit methods. This behavior cannot be observed in the other explicit methods.

Testing Implicit Methods

Opposite to the case of explicit methods, for linear problems implicit methods count with an extensive stability region which does not make their stability dependent on the value of the step k. The problem was simulated using Implicit Euler, BDF2 with Fixed Point as corrector and BDFk with Newton as corrector for k between 1 and 4. All the following experiments take as initial value
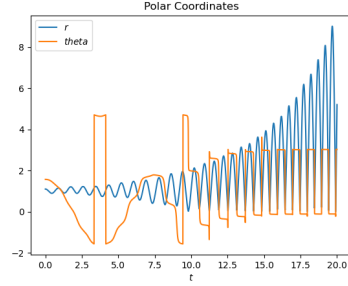
3

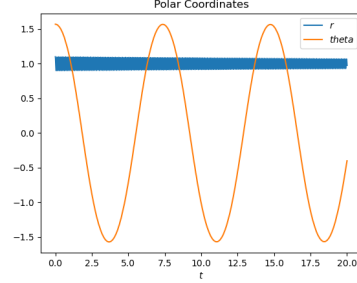Figure 7: Explicit Euler $h = 0.01$ $k = 50$
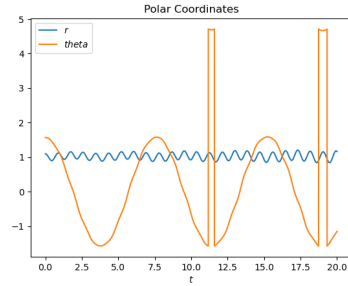

Figure 8: RK4 $h = 0.01$ $k = 3000$

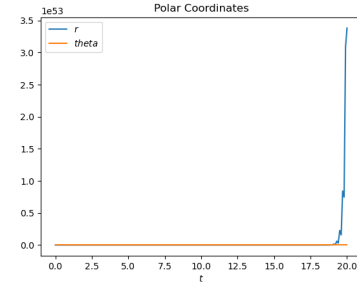Figure 9: Explicit Euler $h = 0.001$ $k = 50$

Figure 10: RK4 $h = 0.1$ $k = 975$

$y_0 = [1.1, 0, 0, 0]$ and have $[0, 20]$ for time domain. It is interesting to see how the oscillation of the spring decays for implicit methods. This decay can be attenuated by reducing the step size or accelerated by increasing the value of the spring constant.

The method BDFk with Newton presents a decay in the spring oscillation as the other methods do. However, it also shows decay of the pendulum oscillation which cannot be observed in the other implicit methods. To better observe this decay (Figure 15 and Figure 16) the domain is increased to $[0, 100]$.

It is interesting to see how the relation between the speed of decay of the spring oscillation in inversely proportional to the size of the stability region of the methods tested.
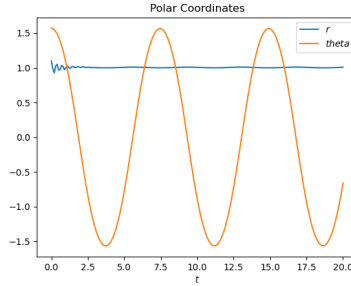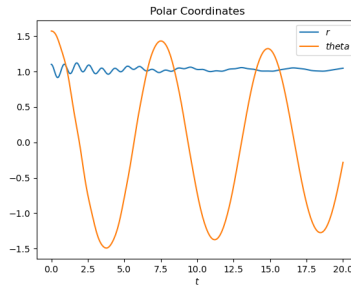
Figure 11: RK4 $h = 0.1$ $k = 300$

Figure 12: Implicit Euler $h = 0.01$
$k = 50$

Testing CVODE

A first test series

In the first specific test of CVODE we solve our toy problem for increasing k. Here we switch between the BDF and Adam-Moultons discretisation method. We also vary the `maxorder` parameter for both methods. A higher k reflects a problem which is more stiff. As a stiff problem requires smaller steps the number of steps `nsteps` increases as k increases which can be seen in figure 17. As the number of function evaluations per stepsize `nfcns`/`nsteps` hovers slightly above 1 for all methods (c.f. figure 19) the number of function evaluations increase proportionally to `nsteps` with k as can be seen in figure 18. There is however a difference in how many steps each method needs. The BDF-method requires in general more steps than the Adams-Moulton method. And the general trend is that the number of steps increases as `maxord` is reduced.

From figure 20 it can be seen that the number of jacobian evaluations stays roughly constant and happens roughly every 5th step. The number `nerrfails`/`steps` stays roughly constant in dependence of k though the general tendency is that it is smaller the lower `maxord` is set. This makes sense because a lower
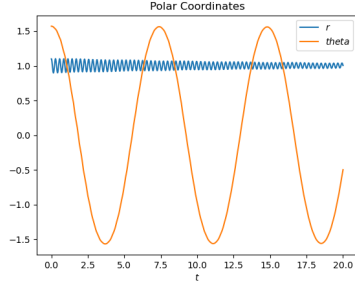
5

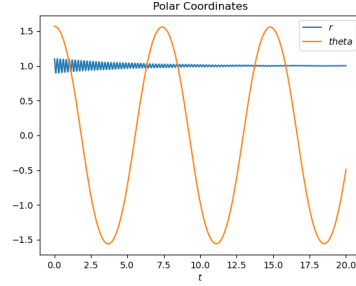Figure 13: BDF2-Fixed Point
$h = 0.001$ $k = 500$

Figure 14: BDF2-Fixed Point
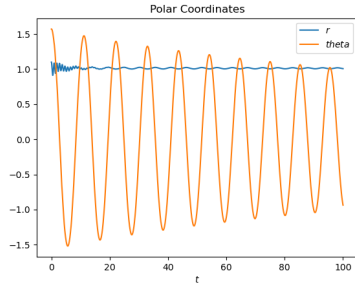$h = 0.01$ $k = 1000$
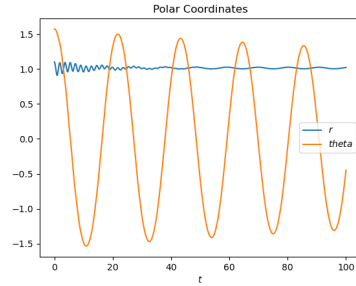

Figure 15: BDF2-Newton $h = 0.01$
$k = 100$

Figure 16: BDF4-Newton $h = 0.01$
$k = 100$

`maxord` means there are fewer possibilities for the method order and hence fewer
changes of order. In figure 22 we see a difference in how much the methods obey
the principles of energy conservation. One can see that for growing k the result
tends to be further away from physical reality. Once again the methods with
higher `maxord` do better with the exception of the BDF method where for some
reason a `maxord` of 4 performs best.

This test confirms once again that a stiffer Problem needs more function
evaluations in CVODE. Perhaps surprisingly the Adams-Moulton-method seems
to perform better on this problem. This experiment also highlights that a lower
`maxord` parameter tends to be more computationally expensive though it reduces
the number of error test failures `nerrfails`.

Testing the parameter rtol

We now test the influence of the parameter `rtol` on the methods BDF and
Adams-Moulton. For this we set $k = 10^3$ and keep all other parameters on their
default values. The results can be seen in figures 23 to 27. We note that as `rtol`
increases the number of steps decreases (c.f. figure 23). If one compares figures
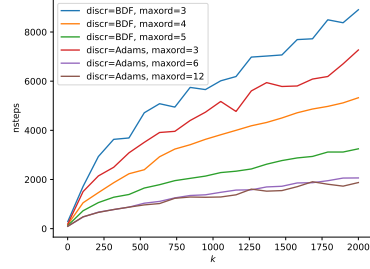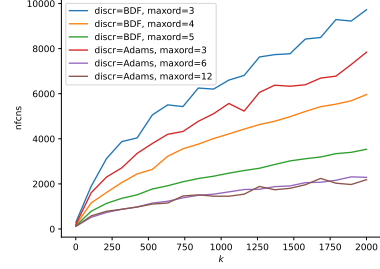
6

Figure 17: `nsteps` in relation to the parameter k.

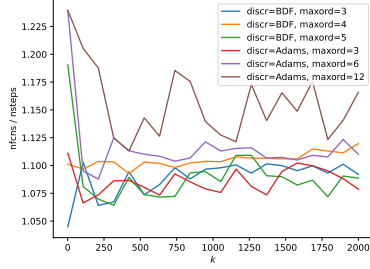

Figure 18: `nfuncs` in relation to the parameter k.

Figure 19: `nfcns`/`nsteps` in relation to the parameter k.
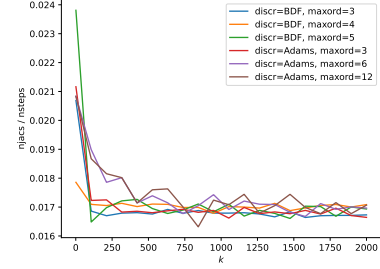

Figure 20: `njacs`/`nsteps` in relation to the parameter k.

the instability index for $k \approx 10^3$ in figure 22 with the instability index in figure 27 one sees that changing the `rtol` parameter from the default makes the result significantly worse in terms of energy conservation.

Testing the parameter atol

If we test the `atol` parameter on the Adams and Newton method analogously to the test of the `rtol` parameter we once again get an instability index that is significantly above the value for the method in which we did not specify this value as can be seen in Figure 28. In either case we observe that fixing the tolerance seems to come at the cost of energy conversation as is dramatically visualised in Figures 29 and 30.

All in all we see that none of the (admittedly crude) tweaking of the parameters improved the performance of CVODE. To the contrary, most changes worsened the performance. The choice of the discretisation method on the other hand did make a big difference and the performance for solving the toy problem could be improved by switching from the default BDF method.
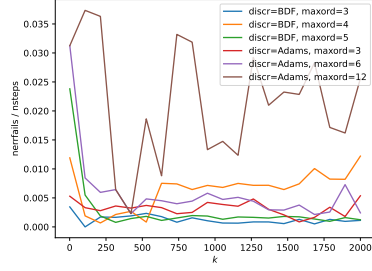
Figure 21: `nerrfails/nsteps` in relation to the parameter k.

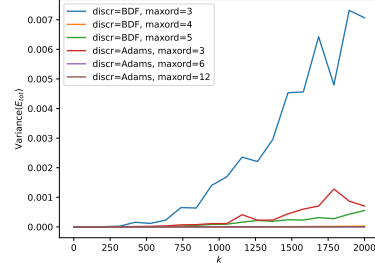Figure 22: instability index in relation to the parameter k.

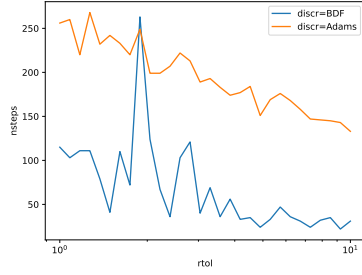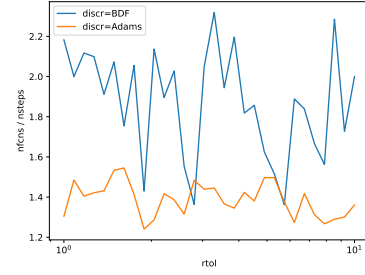Figure 23: `nsteps` in relation to the parameter `rtol`.

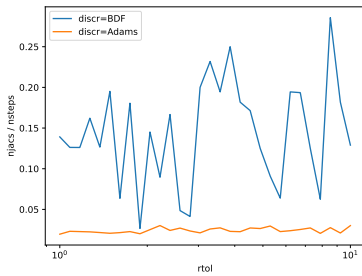Figure 24: `nfcns/nsteps` in relation to the parameter `rtol`.

Figure 25: `njacs/nsteps` in relation to the parameter `rtol`.
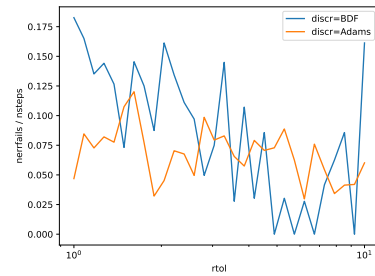

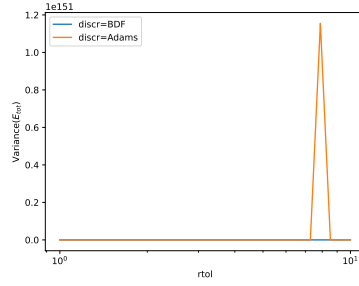Figure 26: `nerrfails/nsteps` in relation to the parameter `rtol`.

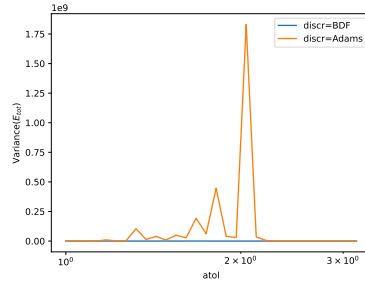Figure 27: instability index in relation to the parameter `rtol`.

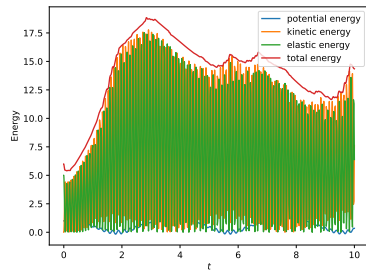Figure 28: instability index in relation to the parameter `atol`.

Figure 29: Energy plot for $k = 10^3$ with `atol=1E-2`.
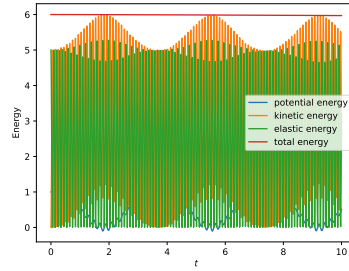

Figure 30: Energy plot for $k = 10^3$.

Project 2

In this project we used the implementation of the seven body mechanism as described in [3] to test Assimulo's implicit solvers. The problem formulation leads to an index 3 problem of the form

$$M(q) \, q'' = f(q, q') - G(q)^\top \lambda \tag{1}$$
$$0 = g(q) \tag{2}$$

where $q \in \mathbb{R}^7$, $\lambda \in \mathbb{R}^6$ and $G = Dg$. If we differentiate condition (2) we obtain the index 2 condtition

$$0 = G(q) \, q'$$

and differentiating this again we obtain the index 1 formulation

$$0 = \partial_q^2 g(q) \, (q', q') + G(q) \, q'' \, .$$

Note that condition (??) and (1) can be uniquely solved for q'' and λ and we then obtain an ODE in the explicit formulation. For the implementation we rewrite this second order system as a first order system by the usual trick of introducing the variable $v = q'$ so that in the implicit formulation the problem depends on the variable

$$y = \begin{bmatrix} q \\ v \\ \lambda \end{bmatrix}$$

A plot of the solution of the index 1 formulation can be seen in Figures 31 to 33.

Generation of consistent initial values

Given the restrictions imposed over the system the generation of initial values is not a trivial task. To do this we follow the steps presented in the literature, we start with q and v.

First we take $\theta = 0$ which can be done given that the system is undetermined and we assume a solution exists (this makes sense as a physical model of the
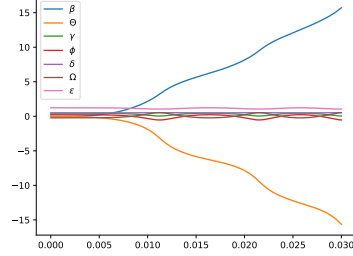
10

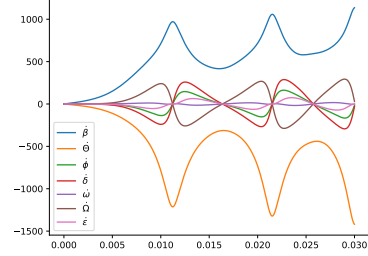Figure 31: The angles of the solution to the index 2 problem.

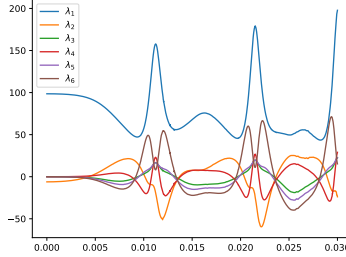Figure 32: The angle speed of the solution to the index 2 problem.

Figure 33: The Lagrange parameter of the solution to the index 2 problem.

system was presented in class). We then use *Newton Iteration* to solve the equations obtaining values for the remaining angles. We also take the initial value of v to be 0 as we assume the system starts at rest. Now for w and λ using the Index 1 formulation we have to solve a linear system which is presented in the literature. Doing this we get the values given in tables 35-36.

Many of the values are minute but non-zero. This is due to rounding errors, but in theory these small values equal zero.

A comparison of the index 1, 2 and 3 formulations

We now would like to compare the solutions of the various formulations. To calculate the solutions we used the IDA solver (TODO: hyperlink). However, to get the problem to run we set the `atol` parameter to the large number `1E5` and the `algvar` parameter to `False` for the algebraic variable λ and for v. These settings remain unchainged and in the following we only vary the index of the problem. We can see in the figures 37 to 39 the difference of the index 1 solution

β	-0.0617139
Θ	0
γ	0.45528
ϕ	0.222668
δ	0.487365
Ω	-0.222668
ϵ	1.23055

Figure 34: Consistent initial angles

$\ddot{\beta}$	14222.4
$\ddot{\Theta}$	-10666.8
$\ddot{\phi}$	7.58763e-14
$\ddot{\delta}$	1.53229e-13
$\ddot{\omega}$	-1.71547e-14
$\ddot{\Omega}$	-1.53229e-13
$\ddot{\epsilon}$	5.79407e-14

Figure 35: Consistent initial accelerations

λ_1	98.5669
λ_2	-6.12269
λ_3	2.2899e-17
λ_4	-1.87294e-17
λ_5	3.37745e-17
λ_6	4.83113e-17

Figure 36: Consistent initial lambdas

subtraced from the index 3 solution. In the figures 40 to 42 we see the index 2 solution subtracted from the index 3 solution. As expected we see that the difference the solutions grows as time progresses.
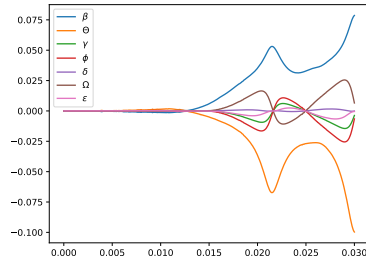

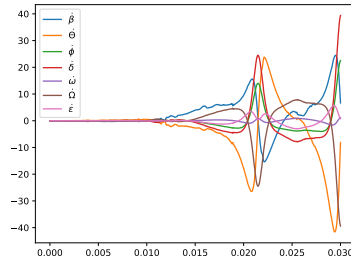Figure 37: The difference of angles of the index 1 and the index 3 solution.

Figure 38: The difference in angle speeds of the index 1 and the index 3 solution.

Rather unexpectedly however the difference of the index 1 to the index 3 solution is in general greater than the difference of the index 2 to the index 3 solutions. Also unexpectedly these differences are noticable in the plots of the Lagrange parameter λ as shown in figures 43, 44 and 33. Here we see that the solution becomes increasingly rough as the index increases.

The performance of the IDA solver for the various indexes can be seen in figures 45 to 48. We see figure 45 that the number of steps of the solver increases with the index. As the number of function evaluations per step stays roughly constant by figure 46 this means that the number of function evaluations increases with the index. One other other notable statistic regards the number of error test failures for the different problems which can be seen in figure 48 where we see a larger difference between the problems though this is probably not statistically significant as the total number of error test failures is approximately a dozen.
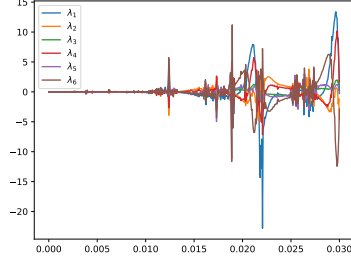
Figure 39: The difference of lambdas of the index 1 and the index 3 solution.
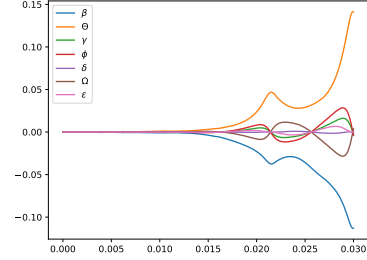

Figure 40: The difference of angles of the index 2 and the index 3 solution.
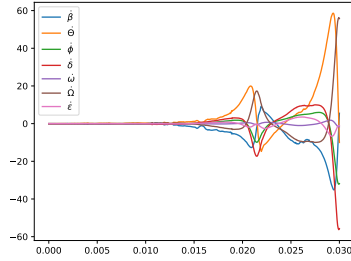

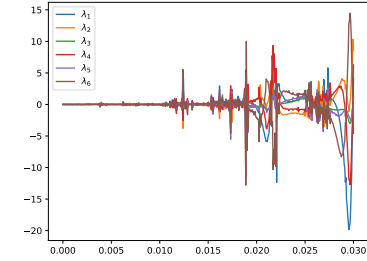Figure 41: The difference in angle speeds of the index 2 and the index 3 solution.

Figure 42: The difference of lambdas of the index 2 and the index 3 solution.

Dependence on the parameters `algvar` and `atol`

As previously indicated the IDA solver will throw an error

```
assimulo.solvers.sundials.IDAError: 'Convergence test failures
                                    occurred too many times during
                                    one internal time step or minimum
                                     step size was reached. At time 0
                                    .000000.'
```

This can be resolved by declaring the entries of y corresponding to v and or λ to be algebraic variables with the parameter `algvar` and to set the parameter `atol` to a large variable. In the following we would like to check how these parameters impact the performance of the solver in the case of the index 1 formulation. For this we denote by `algvar_v` and `algvar_lambda` the value of the `algvar` parameter for v and λ. The default value of `algvar` is set to True. Analogously we denote the components of `atol` corresponding to v and λ with `atol_v` and `atol_lambda` and set the default value to `1E-6`. We now run a
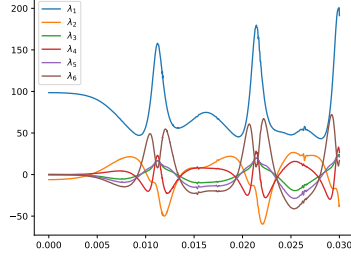
13

Figure 43: The Lagrange parameter of the index 2 problem.

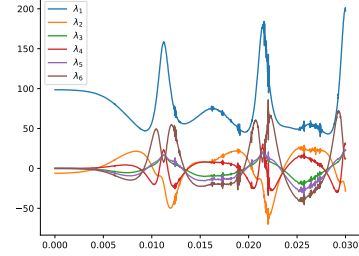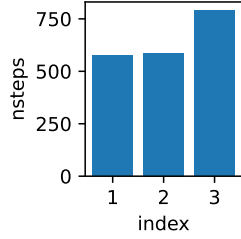Figure 44: The Lagrange parameter of the index 3 problem.
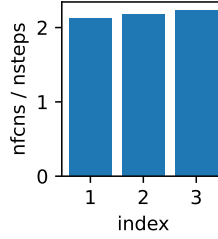

Figure 45: `nsteps` in relation to the index.
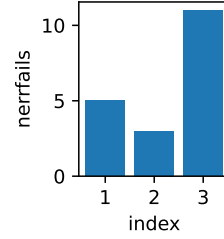

Figure 46: `nfcns/nsteps` in relation to the index.

Figure 47: `nerrfails` in relation to the index.

series of 5 experiments as depicted in table 49.

As all experiments deliver more or less the same result we will be comparing the statistics of IDA as depicted in figures 50 to 55. Once again we observe in figure 53 that the total number of function evaluations is roughly proportional to the number of steps needed. Here experiments 1 and 4 stick out for requiring comparatively more function evaluations per step. However in figure 50 we see that these are also precisely the experiments in which the total number of steps taken is by far the least. Experiments 1 and 4 are also precisely those experiments that have the most stringent requirements on the v part of y. Both have set `atol_v=1E-6` and declare v to not be an algebraic variable. We see in figures 52 and 55 that experiment 0 is an outlier in requiring comparitively many jacobian evaluations and having relatively few error test failures.

Using an explicit method

As part of the final task we used an explicit RK4 method to solve the index 1 problem. As a result of the method exploding for $h = 0.01$, the default step
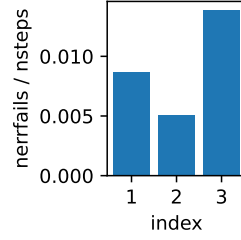
Figure 48: `nerrfails` `/nsteps` in relation to the index.

experiment	index	atol_v	atol_lambda	algvar_v	algvar_lambda	suppress_alg
0	1	100000	100000	False	False	True
1	1	1e-06	100000	False	True	True
2	1	1e-06	100000	True	False	True
3	1	1e-06	100000	True	True	False
4	1	1e-06	1e-06	False	False	True

Figure 49: Parameters in the experiments

value, the method was tested for various values of h.

In particular in Figure ... the L_2 norm of each angle over time is plotted with respect to $h \in [0.001, 0.002)$ with $\Delta h = 5e-6$.

The explicit method can then be tested with individual step sizes and as expected, the method explodes for $h \in \{0.001446, 0.0018, 0.00195\}$ and is stable for $h \in \{0.00185, 0.0012, 0.0016\}$.

In Figures ... and ... it can be observerd the aproximation using the explicit RK4 for a value of the stes size which makes the approximation stable, in particular we are taking $h = 1e-4$.
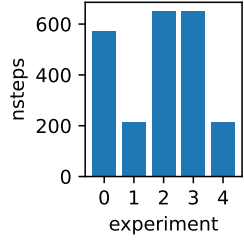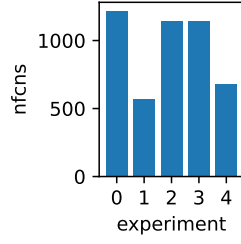
Figure 50: `nsteps` of the experiments.

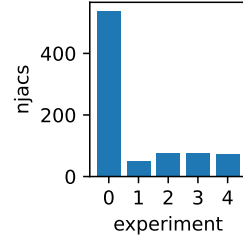
Figure 51: `nfcns` of the experiments.
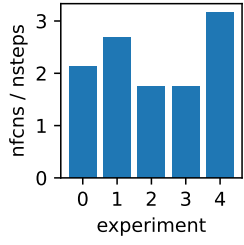

Figure 52: `njacs` of the experiments.
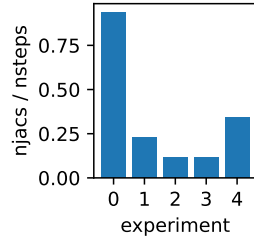

Figure 53: `nfcns/nsteps` of the experiments.

Figure 54: `njacs/nsteps` of the experiments.
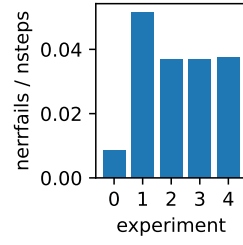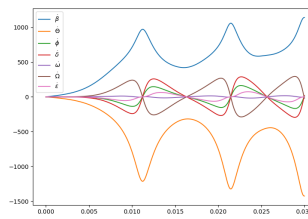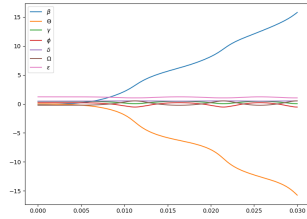

Figure 55: `nerrfails/nsteps` of the experiments.

Project 3

In this project we consider an initial value problem of the form

$$M\ddot{u} + C\dot{u} + Ku = f(t)$$
$$u(0) = u_0$$
$$\dot{u}(0) = v_0$$

for this we implemented an Assimulo problem class, the HHT solver and the Newmark implicit and explicit solvers. The explicit solver was tested on the pendulum

The pendulum revisited

An elastic beam

In the second part of the project we tested the implicit Newmark and the HHT method on a discretised beam as seen in figure 56. The beam is displaced by a force until it is deformed as in figure 57. With time it then swings back and forth between the positions in figures 56-59. Figure 60 shows the displacement of the tip of the beam in dependence of time.
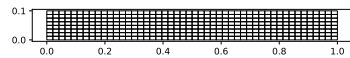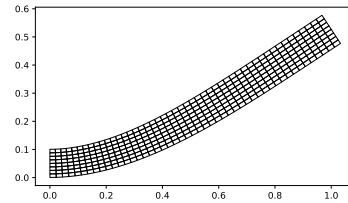

Figure 56: Beam position at $t \approx 0$.

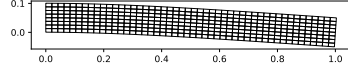Figure 57: Beam position at $t \approx 1.7$.
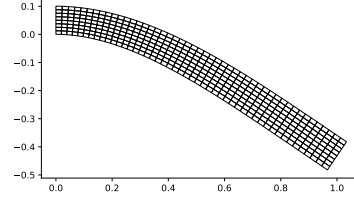
17

Figure 58: Beam position at $t \approx 2.4$.

Figure 59: Beam position at $t \approx 2.7$.

We can calculate the elastic and kinetic energies according to the formulas

$$E_{\mathrm{kin}} = \frac{1}{2} v^\top M v \qquad\qquad E_{\mathrm{elast}} = \frac{1}{2} u^\top C u$$

which add up to the total energy

$$E_{\mathrm{tot}} = E_{\mathrm{kin}} + E_{\mathrm{elast}}$$

The development of the energy of the system can be seen in figure 61. Here we see in particular that after the initial application of an external force to the system the energy stays almost constant. As in project 1 the variance of the total energy serves as a measure of the instability of the solver. Here we calculate this variance only for the latter 4/5 of the simulation because in the first part the applied force changes the total energy. With an ideal solver this quantity vanishes.
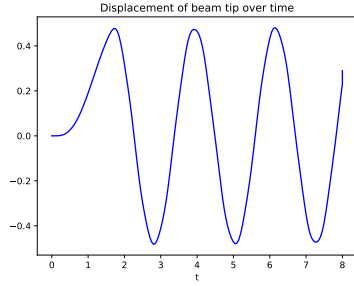

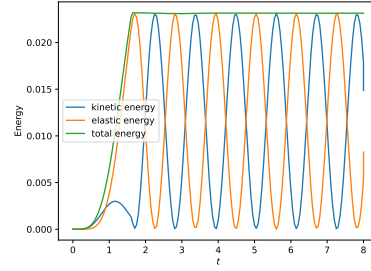Figure 60: Displacement of the tip of the beam of the solution.

Figure 61: Energy in dependence of time of the solution.

A brief comparison of solvers

In a first experiment we compare the performance of our implementation of the HHT solver and the implicit Euler solver from Assimulo. The HHT method

18

was applied with the parameter $\alpha = 0$ and the stepsize was the same for all methods. The results are plotted in figure 62. Here one sees that for all solvers the variance of the total energy is small. There is however a big difference in the performance of the various methods. On my computer the implicit Euler solver takes roughly two orders of magnitude longer than the HHT method.

solver	HHT	ImplicitEuler
Variance(E_{tot})	0	0
Elapsed simulation time [s]	1.2	226.6

Figure 62: Performance of various solvers for the beam problem

Testing the implicit Newmark solver

In a second experiment we test the dependence of the implicit Newmark method on the parameters β and γ whereby we keep the parameter $\alpha = 0$ and the stepsize $h = 0.05$ constant. The variance of the total energy can be seen in figure 63. It should be noted that we cut off the value of the variance of the total energy at 10^2 because this value shows that the solution is instable for the specific choice of β and γ. One can observe that the problem becomes more stable with decreasing β and and that the region of stability increases with decreasing γ. Figure 64 shows what happens if we leave the region of stability.
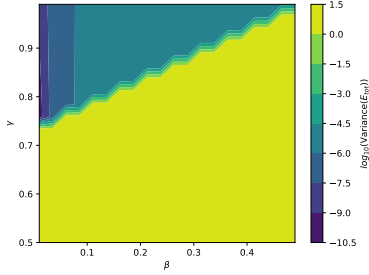

Figure 63: Dependence of the variance of the total energy on the parameters β and γ for $\alpha = 0$.
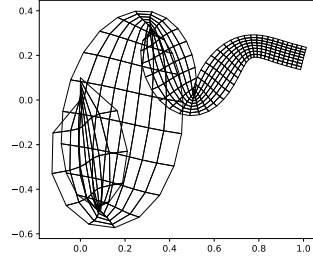

Figure 64: The parameter choice $\beta = 0.25$ and $\gamma = 0.7$ yields a rather peculiar beam configurations.

Testing the HHT solver

In a final experiment we test the dependence of the HHT solver on the parameter α. The variance of the total energy can be seen in figure 65 where it is noticable that the value decreases as α increases albeit from a small level. To make it more visible what is happening we set the step size to $h = 1$ and plotted the energies of the solutions for the HHT solver as can be seen in figures 66 and

67. Here the parameter $\alpha = -1/3$ acts in a dampening manner in comparison to the plot for $\alpha = 0$. It is also astonishing that despite the very rough step size the energy plot for $\alpha = 0$ shares many features of the solution with a more refined step size, like the almost constant total energy and the eventual periodic behaviour of the kinetic and elastic energies.
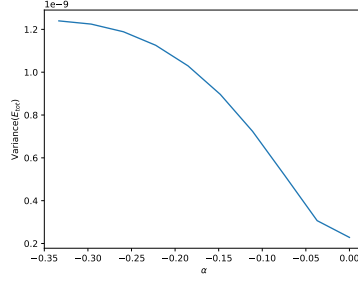

Figure 65: Dependence of the variance of the total energy on the parameter α.
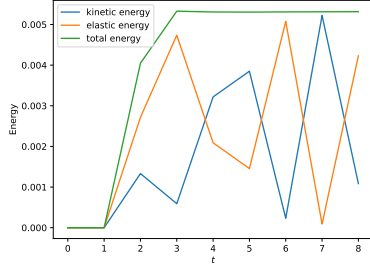

Figure 66: Energy f1or the HHT method with $\alpha = 0$ and stepsize $h = 1$.
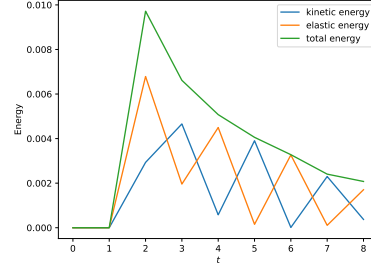

Figure 67: Energy for the HHT method with $\alpha = -1/3$ and stepsize $h = 1$.
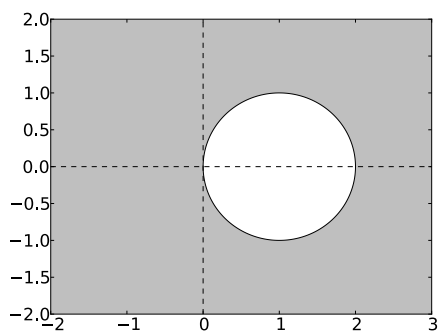
Appendix

Figure 68: Stability region for BDF1, taken from [1]
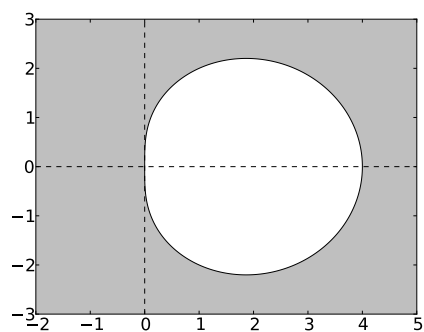

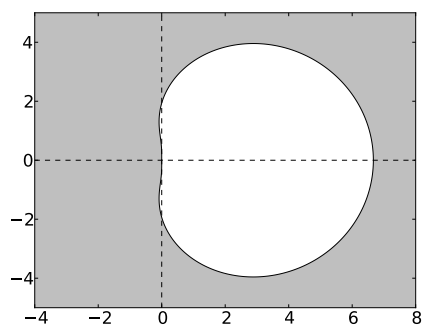Figure 69: Stability region for BDF2, taken from [1]

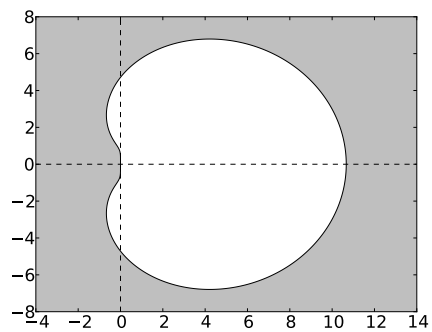Figure 70: Stability region for BDF3, taken from [1]

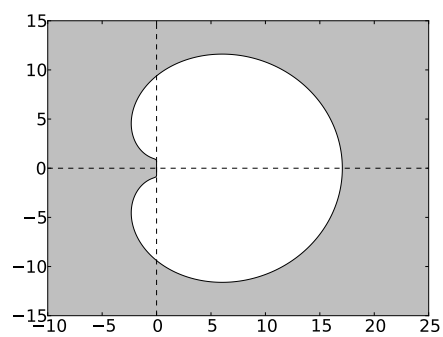Figure 71: Stability region for BDF4, taken from [1]

21

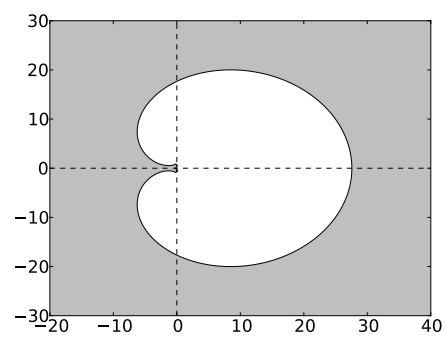Figure 72: Stability region for BDF5, taken from [1]

Figure 73: Stability region for BDF6, taken from [1]

Bibliography

[1] Backward differetiation formula. *Estimation lemma — Wikipedia, The Free Encyclopedia.* Online; accessed 27-January-2023. 2022. URL: `https://en.wikipedia.org/wiki/Backward_differentiation_formula`.

[2] Peter Deuflhard and Folkmar Bornemann. *Numerische Mathematik 2.* revised. de Gruyter Lehrbuch. [de Gruyter Textbook]. Gewöhnliche Differentialgleichungen. [Ordinary differential equations]. Walter de Gruyter & Co., Berlin, 2008, pp. xii+499. ISBN: 978-3-11-020356-1.

[3] E. Hairer and G. Wanner. *Solving ordinary differential equations. II.* Vol. 14. Springer Series in Computational Mathematics. Stiff and differential-algebraic problems, Second revised edition, paperback. Springer-Verlag, Berlin, 2010, pp. xvi+614. ISBN: 978-3-642-05220-0. DOI: `10.1007/978-3-642-05221-7`. URL: `https://doi-org.ludwig.lub.lu.se/10.1007/978-3-642-05221-7`.

[4] simulation-tools-VT23. *Github repository to the project.* Online. 2023. URL: `https://github.com/TheoKoppenhoefer/simulation-tools-VT23`.